PROCEEDINGS OF SCIENCE

Measurements of rare electroweak processes including vector boson scattering and tri-boson production with ATLAS

Vadim Kostyukhin, on behalf of the ATLAS Collaboration[a,*]

[a] *Center for Particle Physics Siegen (CPPS), Department Physik, Universität Siegen, 57068 Siegen, Germany*

E-mail: vadim.kostyukhin@cern.ch

Measurements of rare processes in the electroweak sector provide unprecedented constraints on the SM theory, and unique sensitivity to study the electroweak symmetry breaking and the quartic boson self-couplings. This proceeding presents recent ATLAS measurements of electroweak di-boson production in the vector boson scattering process (VBS) and tri-boson VVZ production using 140 fb^{-1} of data collected at LHC in Run 2 at $\sqrt{s}$ = 13 TeV. In addition to cross-section measurements, studies of boson polarisation states in the VBS process are being actively pursued to bring further sensitivity to new phenomena. First evidence for longitudinally polarised W bosons in the VBS production of the same-sign W boson pairs is presented, also based on the 140 fb^{-1} of data collected by ATLAS in Run 2 at LHC.

The European Physical Society Conference on High Energy Physics (EPS-HEP2025)
7-11 July 2025
Marseille, France

*Speaker

 ISSN 1824-8039 . Published by SISSA Medialab.

PoS(EPS-HEP2025)289

1. Electroweak VVZ tri-boson production

In the Standard Model (SM), the non-Abelian structure of the electroweak sector predicts self-interactions of vector bosons, leading to vertices with three or four vector bosons. Studying processes containing such vertices is a sensitive test of the SM, as deviations from the SM expectation would be hints of new physics. Representative Feynman diagrams for the production of three massive vector bosons are shown in Figure 1.

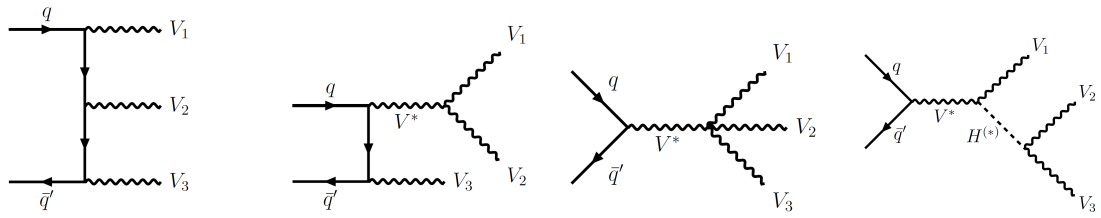

Figure 1: Leading-order representative Feynman diagrams for the production of three massive vector bosons.

This proceeding describes an ATLAS [1] search for the production of three massive vector bosons, of which at least one is a Z boson (WWZ, WZZ, ZZZ) [2], using 140 fb^{-1} of data collected in Run 2 of the LHC. Three search channels are used, namely $3l$ for WWZ and WZZ, $4l$ for WWZ, and at least $5l$ for the WZZ and ZZZ processes, with $l = e, \mu$. In total, seven signal regions (SRs) are defined, targeting different tri-boson systems, namely three SRs for $3l$ and $4l$ states and one SR for the $5l$ state. Five control regions (CRs) are defined in addition to control ttZ, Z+jets and di-boson backgrounds. The signal and background contributions in all SRs and CRs are shown in Figure 2 together with the observed data events. To separate the signal from the background, seven independent classification BDTs are trained, one for every SR.

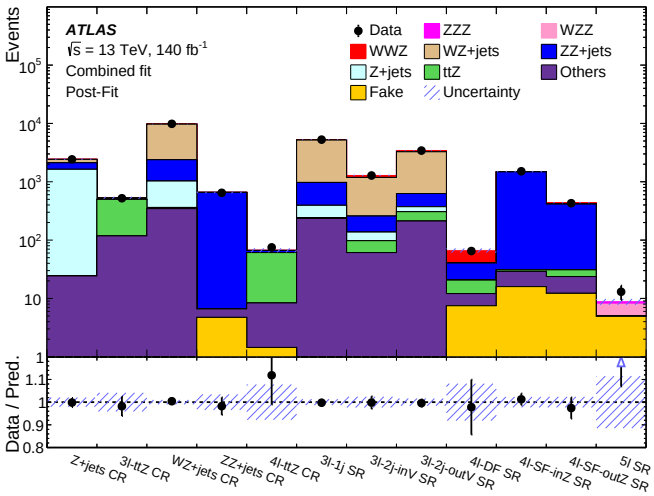

Figure 2: Predicted yields together with the observed number of events for all SRs and CRs [2]. The bottom panel shows the ratio of the data and SM predictions.

The SR BDT scores and CR sensitive variables are combined in the profile likelihood fit to

measure the tri-boson production cross sections. Table 1 shows the measured signal strengths, cross sections and observed (expected) sensitivities for the VVZ, WWZ, and WZZ processes. The ZZZ process is not measured separately due to a smaller cross-section and insufficient data amount.

Table 1: Measured signal strengths, inclusive cross sections and observed (expected) sensitivities for VVZ, WWZ, and WZZ production [2].

Process	Signal strength	Cross section (fb)	Observed (expected) sensitivity
VVZ	$1.43 \pm 0.20(\text{stat.})^{+0.21}_{-0.19}(\text{syst.})$	$660^{+93}_{-90}(\text{stat.})^{+88}_{-81}(\text{syst.})$	6.4 (4.7) σ
WWZ	$1.33 \pm 0.28(\text{stat.})^{+0.21}_{-0.17}(\text{syst.})$	$442 \pm 94(\text{stat.})^{+60}_{-52}(\text{syst.})$	4.4 (3.6) σ
WZZ	$2.13^{+1.18}_{-0.96}(\text{stat.})^{+0.76}_{-0.41}(\text{syst.})$	$200^{+111}_{-91}(\text{stat.})^{+65}_{-37}(\text{syst.})$	2.8 (1.6) σ

The production of three massive vector bosons allows for the study of quartic vector boson vertices. The Wilson coefficients of the most sensitive operators in massive tri-boson final states are f_{M2}, f_{M3}, f_{M4} and f_{M5}. The unitarity bounds of the Wilson coefficients are estimated by adapting the existing calculation for dimension-8 operators in two-to-two scattering processes into vector boson scattering processes and setting the parton centre-of-mass energy $\sqrt{s}$ to the maximum of the three di-boson invariant mass combinations $\max(M_{V_iV_j})$. The observed limits are shown in Table 2.

Table 2: Observed and expected unitarised limits on dimension-8 operator Wilson coefficients, together with the energy scales at which the unitarity bounds are crossed [2].

Coefficient	Expected limit [TeV^{-4}]	Exp. $\sqrt{\hat{s}_c}$ [TeV]	Observed limit [TeV^{-4}]	Obs. $\sqrt{\hat{s}_c}$ [TeV]
f_{M2}/Λ^4	$[-18, 17]$	1.2	$[-19, 19]$	1.2
f_{M3}/Λ^4	$[-28, 29]$	1.5	$[-28, 29]$	1.5
f_{M4}/Λ^4	$[-14, 14]$	1.6	$[-12, 12]$	1.7
f_{M5}/Λ^4	$[-11, 11]$	2.1	$[-9.1, 9.3]$	2.2

2. Longitudinally polarised W bosons in the same-sign WW production in VBS process

The longitudinal polarisation states of the W and Z bosons are generated in the Standard Model by the Goldstone bosons in spontaneous electroweak (EWK) symmetry breaking via the Higgs mechanism. Couplings of the longitudinally polarised W and Z bosons to the Higgs boson prevent a divergence of the tree-level VBS amplitudes at high energies, restoring the unitarity at the TeV scale. The polarised production of the W and Z boson pairs via vector boson scattering (VBS) processes provides a sensitive test of the EWK symmetry-breaking mechanism.

ATLAS search for the polarised production of the same-sign $W^{\pm}W^{\pm}$ pairs uses the leptonic decay modes of the W bosons into electrons or muons [3]. In pp collisions, the VBS processes at leading-order (LO) involve two initial quarks, each of which radiates a gauge boson. They subsequently interact, resulting in the final state with two same-sign leptons, two neutrinos, and

two jets with a large rapidity separation. The electroweak production of $W^{\pm}W^{\pm}jj$ involves only electroweak interaction vertices; representative Feynman diagrams for these processes are shown in Figure 3.

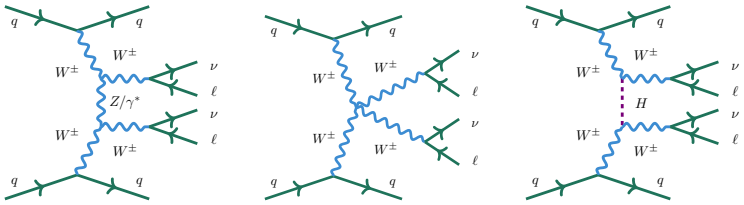

Figure 3: Leading-order Feynman diagrams for the VBS electroweak same-sign W pair production

Electroweak $W^{\pm}W^{\pm}jj$ production can be split into three polarisation components, $W^{\pm}_{\mathrm{L}}W^{\pm}_{\mathrm{L}}jj$, $W^{\pm}_{\mathrm{L}}W^{\pm}_{\mathrm{T}}jj$ and $W^{\pm}_{\mathrm{T}}W^{\pm}_{\mathrm{T}}jj$, where $W^{\pm}_{\mathrm{L}}$ and $W^{\pm}_{\mathrm{T}}$ denote longitudinally and transversely polarized W bosons. The expected contributions of the $W^{\pm}_{\mathrm{L}}W^{\pm}_{\mathrm{L}}jj$ and $W^{\pm}_{\mathrm{L}}W^{\pm}_{\mathrm{T}}jj$ processes are about 10% and 30% of the overall expected electroweak $W^{\pm}W^{\pm}jj$ production cross-section. Differences in the emission, scattering and decay of the $W^{\pm}_{\mathrm{L}}$ and $W^{\pm}_{\mathrm{T}}$ bosons modify kinematic distributions of the final state leptons and jets, which allows for the separation of the different polarisation contributions using deep neural nets (DNN). The limited Run 2 data sample size does not allow for the simultaneous measurement of the three contributions. Therefore, dedicated signal DNNs are trained to separate the $W^{\pm}_{\mathrm{L}}W^{\pm}_{\mathrm{L}}$ state from others and to separate the inclusive $W^{\pm}_{\mathrm{L}}W^{\pm}$ state from the $W^{\pm}_{\mathrm{T}}W^{\pm}_{\mathrm{T}}$. In addition, a VBS process selection DNN is trained to separate the unpolarized electroweak $W^{\pm}W^{\pm}jj$ production from the background processes.

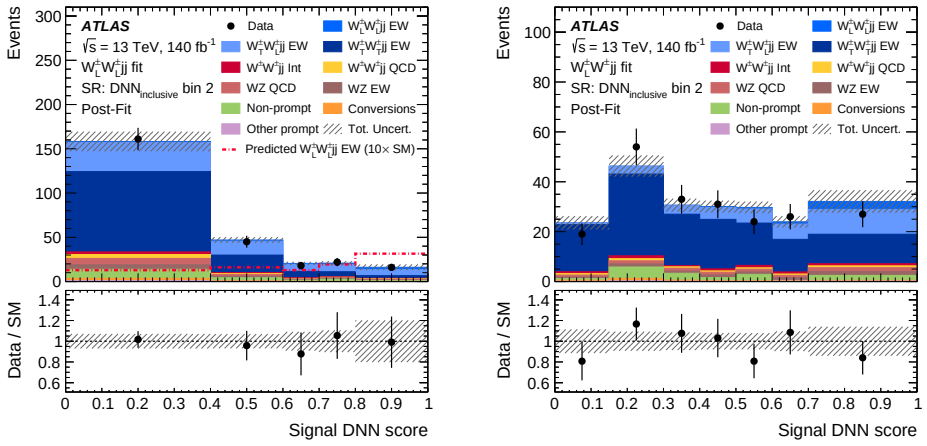

Figure 4: (a) Distributions of the $W^{\pm}_{\mathrm{L}}W^{\pm}_{\mathrm{L}}$ signal DNN score in the region of the VBS selection DNN score values 0.6 to 1 [3]; (b) Distributions of the inclusive $W^{\pm}_{\mathrm{L}}W^{\pm}$ signal DNN score in the region of the VBS selection DNN score values 0.7 to 1 [3].

The observed signal DNN score distributions in the most sensitive signal regions (SRs) are shown in Figure 4. No significant excess of events consistent with $W^{\pm}_{\mathrm{L}}W^{\pm}_{\mathrm{L}}jj$ production is observed. The observed (expected) 95% confidence level upper limit on $\sigma\mathcal{B}(W^{\pm}_{\mathrm{L}}W^{\pm}_{\mathrm{L}}jj)$ is 0.45 (0.70) fb. The significance of the non-zero $W^{\pm}_{\mathrm{L}}W^{\pm}jj$ event yield is quantified assuming contributions only from

the $W_{\mathrm{T}}^{\pm}W_{\mathrm{T}}^{\pm}jj$ process. The observed significance for the $W_{\mathrm{L}}^{\pm}W^{\pm}jj$ process is 3.3σ with an expected significance, evaluated with an Asimov data set, of 4.0σ. The measured cross-sections and the corresponding theoretical predictions from Sherpa3 are summarised in Table 3.

Table 3: Measured and predicted fiducial cross sections for the $W_{\mathrm{L}}^{\pm}W_{\mathrm{L}}^{\pm}jj$, $W_{\mathrm{T}}^{\pm}W^{\pm}jj$, $W_{\mathrm{L}}^{\pm}W^{\pm}jj$ and $W_{\mathrm{T}}^{\pm}W_{\mathrm{T}}^{\pm}jj$ processes [3]. The predicted cross sections from Sherpa3 include NLO EW corrections.

Description	Predicted $\sigma\mathcal{B}$ (fb)	Measured $\sigma\mathcal{B}$ (fb)	Uncertainty breakdown (fb)
$W_{\mathrm{L}}^{\pm}W_{\mathrm{L}}^{\pm}jj$	0.19 ± 0.05	0.16 ± 0.22 (tot.)	± 0.21 (stat.) ± 0.02 (mod. syst.) ± 0.06 (exp. syst.)
$W_{\mathrm{T}}^{\pm}W^{\pm}jj$	2.67 ± 0.66	3.40 ± 0.35 (tot.)	± 0.31 (stat.) ± 0.08 (mod. syst.) ± 0.16 (exp. syst.)
$W_{\mathrm{L}}^{\pm}W^{\pm}jj$	1.24 ± 0.31	0.84 ± 0.37 (tot.)	± 0.35 (stat.) ± 0.05 (mod. syst.) ± 0.11 (exp. syst.)
$W_{\mathrm{T}}^{\pm}W_{\mathrm{T}}^{\pm}jj$	1.62 ± 0.39	2.46 ± 0.37 (tot.)	± 0.34 (stat.) ± 0.06 (mod. syst.) ± 0.14 (exp. syst.)

3. Electroweak di-boson ($WW/WZ/WW$) production study

Standard Model VBS processes involve both the self-couplings of the gauge bosons and their couplings to the Higgs boson. It therefore allows for probing the non-Abelian gauge structure of the electroweak sector of the SM. Study of VBS di-boson production in the semileptonic channel is particularly interesting because it allows to probe the electroweak sector of SM at a higher transverse momentum due to a larger production cross-section. At the LHC, the electroweak di-boson production has two components which cannot be separated in a gauge-invariant way — the VBS and non-VBS ones, as illustrated in Figure 5. To study the VBS component, its contribution must be enhanced via a dedicated event selection.

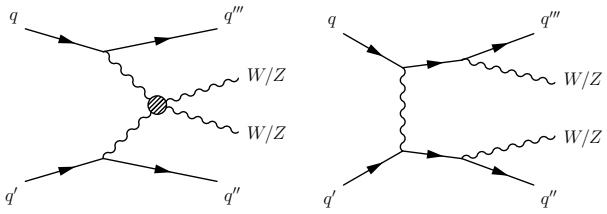

Figure 5: Representative leading order Feynman diagrams for (a) EWK $VVjj$ production via VBS, (b) EWK $VVjj$ production via a non-VBS contribution

This proceeding presents an ATLAS search for the EWK $VVjj$ production in a VBS-enhanced phase space using the semileptonic di-boson decay channel [4]. Events with two forward small-R jets with a high invariant mass are required to have 0, 1 or 2 leptons (e, μ) and a hadronic vector boson candidate identified as a pair of small-R jets or a boosted large-R jet with the invariant mass consistent with the vector boson hypothesis. Nine signal regions (SRs) are defined based on the lepton multiplicity and the boosted high purity, boosted low purity and resolved event topologies. To separate the EWK $VVjj$ process from backgrounds, recurrent neural net (RNN) classifiers are trained in every SR. The analysis design is completed by nine control regions (CRs) for the backgrounds. The combined profile likelihood fit results are shown in Figure 6. The background-only hypothesis is excluded with a significance of 7.4σ, while the expected significance is 6.1σ.

The distributions of events in the SRs are also used to constrain new operators of mass-dimension-8 contributing to anomalous quartic gauge boson couplings, which would enhance

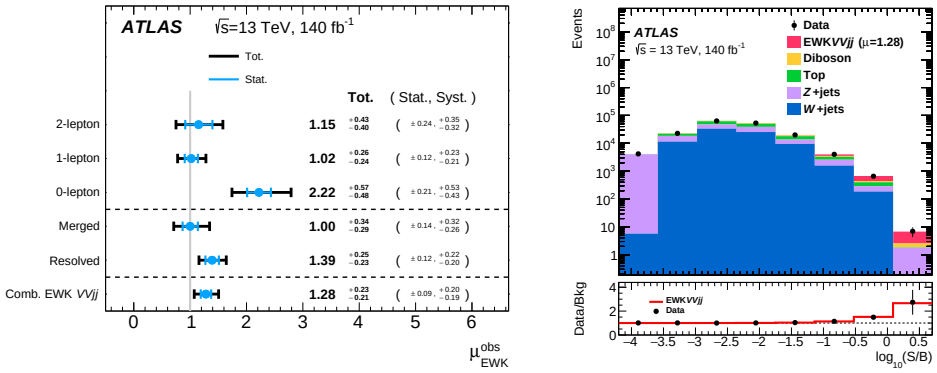

Figure 6: (a) Signal strength μ_{EWK} from the combined profile likelihood fit [4]; (b) Data and predicted SR yields grouped into bins of $\log_{10}$(S/B) to demonstrate a combined signal significance.

EWK VBS production at high di-boson invariant mass. To avoid unitarity violation at high centre-of-mass energy, a running clipping scale E_{clip} is chosen, and signal events with particle-level m_{VV} greater than this clipping scale are removed. The unitarised limits are obtained as crossings of the E_{clip}-dependent limits with the theory unitarity limits for each EFT operator. The expected and observed limits on the different dimension-8 EFT operators are shown in Table 4.

Table 4: Expected and observed 95% confidence interval limits on the Wilson coefficients f_N/Λ^4 of various dimension-8 operators [4]. Limits are obtained considering a single operator at a time.

Wilson coefficient	Expected limit [TeV^{-4}]	Observed limit [TeV^{-4}]	Expected limit unitarized [TeV^{-4}]	Observed limit unitarized [TeV^{-4}]
f_{T0}/Λ^4	[-0.20, 0.18]	[-0.25, 0.22]	[-0.79, 0.47] at [1.76, 1.96] TeV	[-0.85, 0.47] at [1.73, 2.00] TeV
f_{T1}/Λ^4	[-0.19, 0.19]	[-0.24, 0.24]	[-0.34, 0.34] at [2.59, 2.59] TeV	[-0.43, 0.43] at [2.43, 2.43] TeV
f_{T2}/Λ^4	[-0.44, 0.44]	[-0.55, 0.55]	[-0.95, 0.96] at [2.22, 2.22] TeV	[-1.16, 1.17] at [2.12, 2.11] TeV
f_{T3}/Λ^4	[-0.38, 0.38]	[-0.48, 0.48]	[-0.62, 0.62] at [2.71, 2.71] TeV	[-0.88, 0.88] at [2.49, 2.48] TeV
f_{T4}/Λ^4	[-1.46, 1.32]	[-1.51, 1.37]	[-3.03, 2.60] at [2.02, 2.09] TeV	[-3.03, 2.60] at [2.02, 2.10] TeV
f_{T5}/Λ^4	[-0.57, 0.53]	[-0.64, 0.58]	-	[-2.65, 2.57] at [1.53, 1.54] TeV
f_{T6}/Λ^4	[-0.76, 0.72]	[-0.74, 0.71]	[-2.82, 2.01] at [1.66, 1.73] TeV	[-2.98, 2.62] at [1.64, 1.69] TeV
f_{T7}/Λ^4	[-1.78, 1.52]	[-1.94, 1.70]	[-7.88, 4.29] at [1.65, 1.90] TeV	[-6.70, 4.11] at [1.72, 1.91] TeV
f_{T8}/Λ^4	[-0.59, 0.59]	[-0.48, 0.48]	-	-
f_{T9}/Λ^4	[-1.22, 1.22]	[-1.02, 1.03]	-	-
f_{S02}/Λ^4	[-3.22, 3.22]	[-3.96, 3.96]	[-5.53, 5.54] at [2.07, 2.67] TeV	[-6.16, 6.17] at [2.01, 2.01] TeV
f_{S1}/Λ^4	[-6.84, 6.86]	[-8.06, 8.06]	-	-
f_{M0}/Λ^4	[-1.13, 1.12]	[-1.26, 1.25]	[-2.61, 2.58] at [2.00, 2.00] TeV	[-2.71, 2.65] at [1.97, 1.98] TeV
f_{M1}/Λ^4	[-3.23, 3.24]	[-3.95, 3.95]	[-6.22, 6.22] at [2.27, 2.27] TeV	[-7.42, 7.43] at [2.17, 2.17] TeV
f_{M2}/Λ^4	[-1.66, 1.67]	[-1.85, 1.85]	-	-
f_{M3}/Λ^4	[-5.29, 5.29]	[-5.68, 5.71]	[-23.69, 23.39] at [1.57, 1.57] TeV	[-18.62, 19.10] at [1.66, 1.65] TeV
f_{M4}/Λ^4	[-2.62, 2.62]	[-2.96, 2.97]	-	-
f_{M5}/Λ^4	[-3.81, 3.82]	[-4.41, 4.44]	[-6.80, 6.80] at [2.33, 2.33] TeV	[-7.28, 7.30] at [2.29, 2.29] TeV
f_{M7}/Λ^4	[-5.32, 5.20]	[-6.60, 6.43]	[-9.47, 9.38] at [2.43, 2.43] TeV	[-11.91, 11.11] at [2.29, 2.33] TeV

References

[1] ATLAS Collaboration, JINST **3** (2008), S08003

[2] ATLAS Collaboration, Phys. Lett. B **866** (2025), 139527

[3] ATLAS Collaboration, Phys. Rev. Lett. **135** (2025), 111802

[4] ATLAS Collaboration, arXiv:2503.17461 [hep-ex]